JOURNAL OF MATERIALS SCIENCE 17 (1982) 2997–3008

X-ray and electron microscopy studies of polysulphur nitride

R. H. HOEL*, D. J. DINGLEY
H.H. Wills Physics Laboratory, University of Bristol, Bristol UK

$(SN)_x$ crystals have been studied by a combination of scanning electron microscopy, transmission electron microscopy and rotating crystal X-ray diffraction. The studies reveal a structure of considerable complexity. The size of individual crystallites is typically a few nanometres by a few tens of nanometres, and their crystal structure is as previously reported by Mikulski and co-workers rather than that reported by Boudeulle. In bulk crystals there is a mosiac spread of approximately 10° in and about the fibre axis. A new twin mode is proposed where crystals twin about a plane perpendicular to the plane defined by individual chains and is referred to as a $(\bar{1}02)^*$ mode. The possibility of the existence of at least two other twin modes is also discussed. An alternative orientation relationship between the precursor dimer phase and the final polymer is presented.

1. Introduction

1.1. The structure of $(SN)_x$

Polymeric sulphur nitride $(SN)_x$ is an unusual inorganic linear polymer which is metallic from above room temperature down to 0.3 K, where a superconducting transition occurs. Important details of the $(SN)_x$ structure have remained a matter of controversy despite several intensive research programmes. This stems principally from the facts that X-ray structure determinations using powder patterns are confused due to considerable line broadening because of the small diameter of individual needle-shaped crystallites, and because of difficulties in avoiding texture problems. The alternative technique of determining crystal structure by transmission electron microscopy suffers firstly from an inherent lack of precision, secondly because extensive faulting of the crystals renders individual diffraction patterns extremely complicated, and thirdly that there is no satisfactory electron diffraction theory relating diffracted intensities to space-group determination and determination of the position of atoms within the unit cell.

Despite these difficulties, Boudeulle [1] and co-workers applied kinematic electron diffraction theory and reported that $(SN)_x$ had a monoclinic structure with space group $P2_1/C$. Later, independent research by Mikulski and co-workers [2, 3] concluded the same point and space group, but slightly different dimensions of the lattice unit cell and a significant difference in the values of the fractional co-ordinates defining the positions of the atoms within the unit cell. Their values are compared with those obtained by Boudeulle in Tables I and II. The crystals consist of chains of alternating *cis* and *trans* bonds, there being two such chains of two SN groups each per unit cell (Fig 1a, b). The chain axis coincides with the unique crystallographic *b*-axis and the average chain plane is nearly parallel to the $(\bar{1}02)$ plane (Fig. 1c). Boudeulle reported a twinning mode in which the twin was formed by a 180° rotation about the crystal *c*-axis.

As well as the structure described above and termed the β-phase, $(SN)_x$ has been reported to form two other monoclinic phases, termed the α- and α'-phases [1, 4]. The reported lattice constants for the α-phase however, are so similar to those of the β-phase (see Table I) that with the

*Present address: University of California, Berkeley, California, USA.

0022–2461/82/102997–12$03.94/0

TABLE I The unit cell parameters of the $(SN)_x$ α- and β-phases, and the precursor phases. B refers to the Boudeulle structure and M to the Mikulski structure. The number in parenthesis are calculated standard deviations in the last significant figures

		a (nm)	b (nm)	c (nm)	β (degrees)	V (nm^3)
β-phase of $(SN)_x$	Boudeulle	0.412	0.443	0.764	109.5	0.131
	Mikulski	0.4153 (6)	0.4439 (5)	0.7637 (12)	109.7 (1)	0.1325
α-phase of $(SN)_x$		0.404 (5)	0.443 (5)	0.786 (5)	109 (1)	0.133
S_2N_2		0.4485 (2)	0.3767 (1)	0.8452 (3)	106.43 (3)	0.1370
Partially polymerized S_2N_2		0.4460 (4)	0.3755 (4)	0.8470 (9)	105.58 (8)	0.1366

often observed streakiness of the diffraction spots and interference from stacking faults in the structure, it is hard to see how the structures could be distinguished. Boudeulle is alone in observing the α′-structure. This phase she deduces from two irreproducible lines observed in the X-ray powder patterns of some $(SN)_x$ samples.

The purpose of this present study were to ascertain which of the two β structures (Boudeulle or Mikulski) could be assigned to our $(SN)_x$ crystals; to deduce the degree of crystal perfection; and to identify the crystal defects.

1.2. The solid-state polymerization of $(SN)_x$

$(SN)_x$ crystals were prepared in this Laboratory by solid-state polymerization of S_2N_2 [5]. The structure of S_2N_2 is shown in Fig. 2a and b. There is a two-fold screw axis parallel to the crystallographic b-axis. It polymerizes via a partially polymerized phase which has a higher degree of disorder than either the precursor phase or the final polymer phase. The lattice constants of the dimer and monoclinic partially polymerized phases are compared with those of the final polymer α- and β-phases in Table I.

On the basis of the observed structures of the dimer, partially polymerized and final β-phase, Baughman *et al.* [6] were able to predict the reaction mode and the orientational relationship between the polymer and dimer unit cells. They concluded that the dimer polymerizes along its a-axis by S_2N_2 ring opening (Fig. 3).

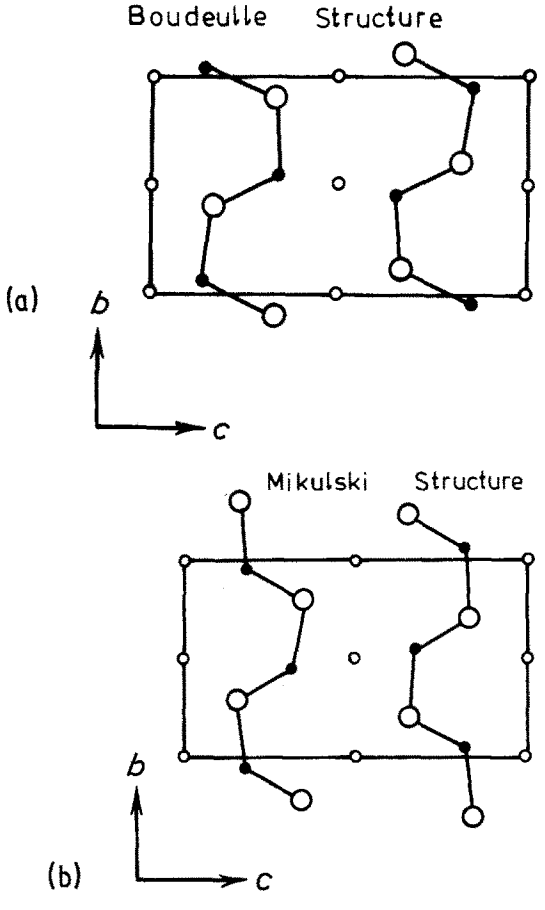

Figure 1 (a) and (b) Boudeulle and Mikulski structures as projected on to the (1 0 0) plane. (c) View along the b-axis of the Mikulski structure. The projection of the Boudeulle structure differs from the Mikulski structure in that the chains are not planar.

TABLE II Positions of the four sulphur and four nitrogen atoms in each unit cell defined by the vectors $X\mathbf{a} + Y\mathbf{b} + Z\mathbf{c}$, $-X\mathbf{a} - X\mathbf{b} - Z\mathbf{c}$, $-Y\mathbf{a} + Y\mathbf{b} - Z\mathbf{c} + \frac{1}{2}(\mathbf{b} + \mathbf{c})$, $X\mathbf{a} - Y\mathbf{b} + Z\mathbf{c} - \frac{1}{2}(\mathbf{b} + \mathbf{c})$. The table lists the values of X, Y and Z for sulphur and nitrogen

	Boudeulle	Mikulski
Sulphur	(0.310, 0.394, 0.168)	(0.179, −0.213, 0.344)
Nitrogen	(0.370, 0.046, 0.146)	(−0.139, −0.069, 0.175)

This ring opening is non-unique in that either of the two centro-symmetrically related bonds shown in the figure may break in the polymerization process. The two chains so formed are related by a 180° rotation about an axis perpendicular to the chain, and perpendicular or parallel to the chain plane. Two such chains constitute the two chains associated with each primitive unit lattice cell shown in Fig. 1.

The predicted orientational relationship between the dimer (d) and polymer (p) unit cells are shown in Fig. 2b and c. It should be noted that the a_d- and b_p-axes coincide; b_d is parallel to c_p and c_d^* parallel to a_p^* (the asterisk refers to the reciprocal lattice axis).

The reaction non-uniqueness and the dimer–polymer orientation relationship discussed above forms the basis for the discussion of structural imperfections in $(SN)_x$, and is of considerable relevance to the present work.

2. Experimental procedure

To study the microstructure of $(SN)_x$, scanning electron microscopy, conventional transmission electron microscopy and rotating crystal X-ray diffraction were applied as experimental techniques.

As-grown, the $(SN)_x$ crystals develop a fibrous structure with the fibre direction coincident with the polymer chain axis. The crystals have a golden lustrous appearance and are mostly of near equidimensional shape, typically a few millimetres across. However, some crystals were also observed in the shape of whiskers or needles, often with

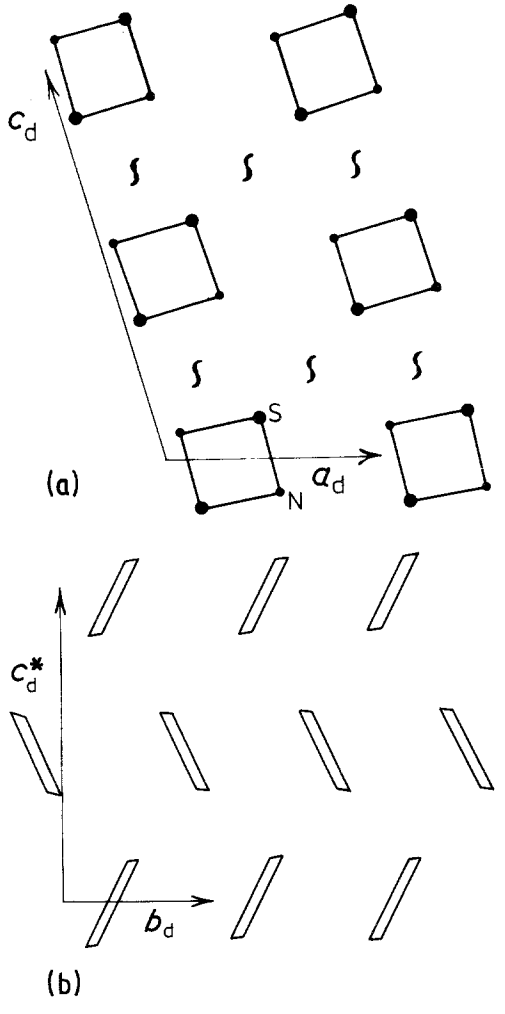

Figure 2 (a) The S_2N_2 structure, projected along the *b*-axis. (b) S_2N_2 structure projected along the *a*-axis. (c) $(SN)_x$ structure in corresponding orientation with dimer phase, showing also twinned structure for twinning about the *c*-axis (———).

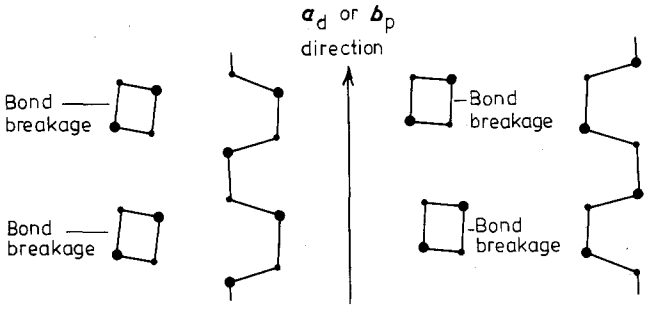

Figure 3 Solid-state polymerization of S_2N_2. The two chains are related by a rotation of 180° about an axis perpendicular to the chain direction.

twisted morphology and typically 0.05–0.2 mm in cross-section and 1–3 mm long.

Untwisted needles, 0.1 mm x 2 mm were chosen for X-ray diffraction studies using the rotating crystal method. The needle direction and hence the polymer chain axis was coincident with the axis of rotation. Important diffraction information was also recorded for crystals held stationary in the camera.

Suitable specimens for transmission electron microscopy were prepared from bulk crystals. The crystals were mechanically stripped and strands typically a few 10 nm thick were detached from the cleaved surface with the aid of sticky electron microscope grids. Attempts in this Laboratory to prepare sections perpendicular to the fibre direction were unsuccessful.

3. Experimental results

3.1. Scanning electron microscopy

The fibrous nature of $(SN)_x$ was clearly revealed in the scanning electron microscope (Fig. 4a). The estimated lateral fibre dimensions from such micrographs vary from 300 down to 100 nm. Transmission electron microscopy (Section 3.3) shows that the crystals are subject to fibrilation

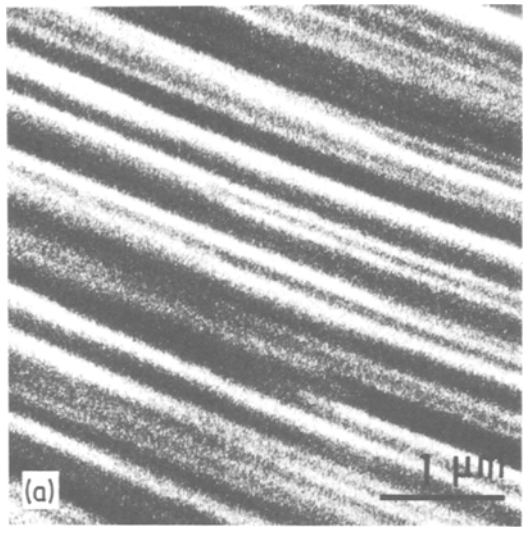

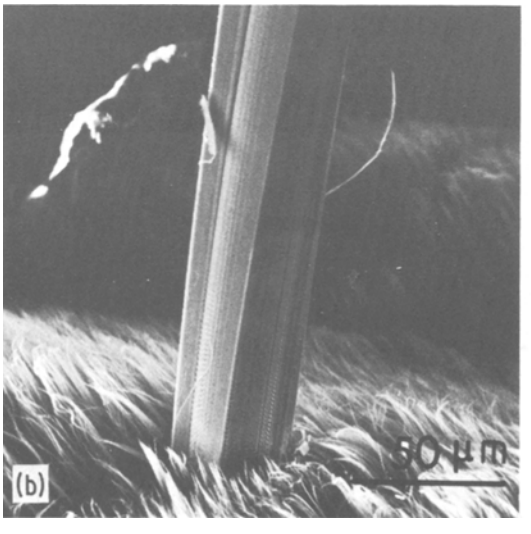

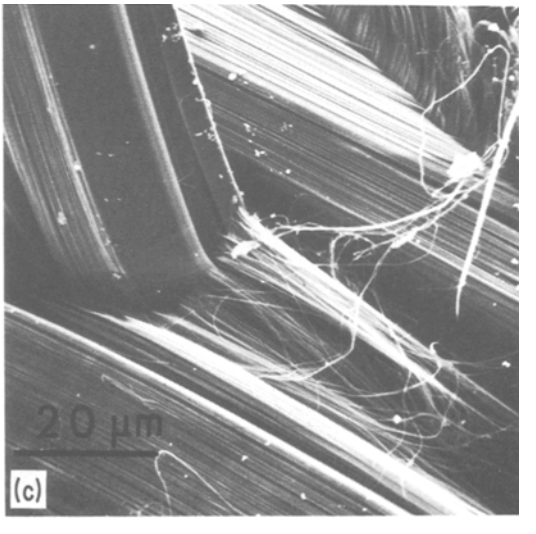

Figure 4 SEM image of (a) an $(SN)_x$ crystal, (b) an $(SN)_x$ whisker growing on a bulk crystal. (c) Whisker growing out of the side face of its parent crystal.

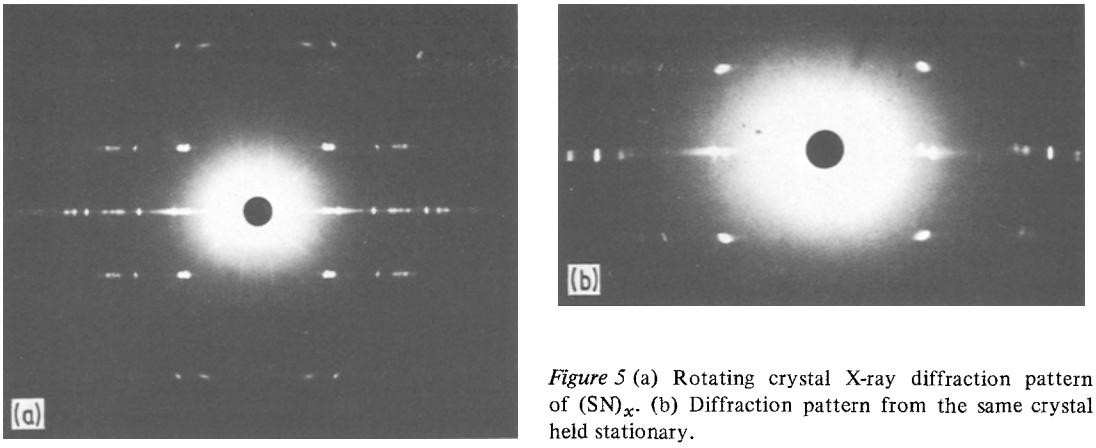

Figure 5 (a) Rotating crystal X-ray diffraction pattern of $(SN)_x$. (b) Diffraction pattern from the same crystal held stationary.

on an even finer scale and strands down to 10 nm have been observed. Considerable unevenness of the end face gives an impression of a high degree of disorder about the fibre axis (Fig. 4b). X-ray diffraction studies (Section 3.2) show that the orientation of these fibres about their axis is not random. Fine whiskers typically 50 μm thick were observed to grow on the bulk crystals and most of these whiskers were of twisted morphology (Fig. 4b). The fibre direction of these whiskers usually differed from that of the bulk crystal. Fig. 4c shows the root of the whisker growing out of the side surface of a crystal making close to 90° with the bulk fibre direction. It is also seen that part of the bulk crystal has a different fibre direction from the rest of it, indicating it is twinned or polycrystalline. The strands of the parent crystal appear disordered near the root of the whisker.

3.2. X-ray diffraction studies

A diffraction pattern from a rotating $(SN)_x$ needle of 0.2 mm cross-sectional dimensions is shown in Fig. 5a. The reflections were indexed according to the monoclinic structure previously reported and the zero layer line periodicities and first and second layer line periodicities are listed in Tables III and IV, respectively. The errors quoted result

TABLE III Zero layer line X-ray reflection periodicities for $(SN)_x$

Observed periodicities (nm)	Possible indices (hkl)	Theoretical peridocities (nm)	
		d_{hkl} Mikulski	d_{hkl} Boudeulle
0.3919 ± 0.0016	100	0.3910	0.3884*
0.3604 0.0016	002	0.3595	0.3601
0.3239 0.0012	$\bar{1}02$	0.3247	0.3233
0.2303 0.0018	102	0.3290	0.2287
0.2025 0.0017	$\bar{2}02$	0.2028	0.2013
0.1965 0.0017	200	0.1955	0.1942*
0.1893 0.0016	$\bar{1}04$	0.1893	0.1892
0.1801 0.0017	004	0.1798	0.1800
	103	0.1792	0.1792
0.1621 0.0016	$\bar{2}04$	0.1624	0.1616
0.1525 0.0015	$\bar{1}05$	0.1527	–
	202	0.1517	0.1511
0.1465 0.0009	104	0.1457	0.1458
0.1311 0.0009	300	0.1303	0.1295*
	203	0.1313	0.1311
0.1269 0.0018	$\bar{3}04$	0.1280	0.1271
	$\bar{1}06$	0.1272	–
0.1204 0.0018	105	0.1223	0.1224
	$\bar{2}06$	0.1222	0.1219
0.1084 0.0018	107	0.1088	–
	$\bar{3}06$	0.1082	0.1078

TABLE IV Some observed first (d_{hkl}) and second (d_{hkl}) layer line periodicities

Observed periodicities (nm)	Possible indices (hkl)	Theoretical Mikulski periodicities (nm)
0.2941 ± 0.0015	110	0.2934
0.2805 0.0024	012	0.2794
0.2042 0.0012	112	0.2035
0.1843 0.0010	212	0.1845
0.1793 0.0010	210	0.1789
0.1739 0.0012	114	0.1742
0.1670 0.0008	113	0.1662
	014	0.1666
0.1950	$\bar{1}21$	0.1942
0.1834 0.0005	122	0.1832
0.1603 0.0010	122	0.1594

from the limited precision with which the specimen to film distance and the exact location of the centre of a reflection could be determined. In Table III, the measured spacings are compared with those obtained by Mikulski and Boudeulle. It is seen that there are three cases where our values and those of Boudeulle differ by more than the estimated errors. These are marked with an asterisk. On the other hand, complete agreement is found between our values and those predicted according to the Mikulski structure. This holds also for the first and second layer lines as shown in Table IV. We observe that all reflections of the form $h0l$ for which $l = 2n + 1$ are absent. This complies with the rule that such reflections are forbidden in the reported space group of this material, $P2_1/C$.

Diffraction patterns from stationary crystals were different from those of a rotating crystal (Fig. 5b), confirming that the fibres grow with preferred orientations about the fibre axis. Reflections were observed, however, which were not expected from a single untwinned crystal, or a crystal containing the c-axis twinning reported by Boudeulle. In Fig. 6 are shown the matrix and c-axis twin zero layer reciprocal lattice nets superimposed. The hatched area in the figure shows the range through which the Ewald sphere has to sweep in order to excite all the reflections observed in Fig. 5b. Clearly therefore, there exist orientations within a single diffracting area other than those of the matrix and c-axis twin. These could arise from other twin modes, twisted fibres and mosaic spread along and between fibres.

3.3. Diffracted X-ray intensities

The zero layer line diffracted intensity profile of an $(SN)_x$ needle is shown in Fig. 7. The observed

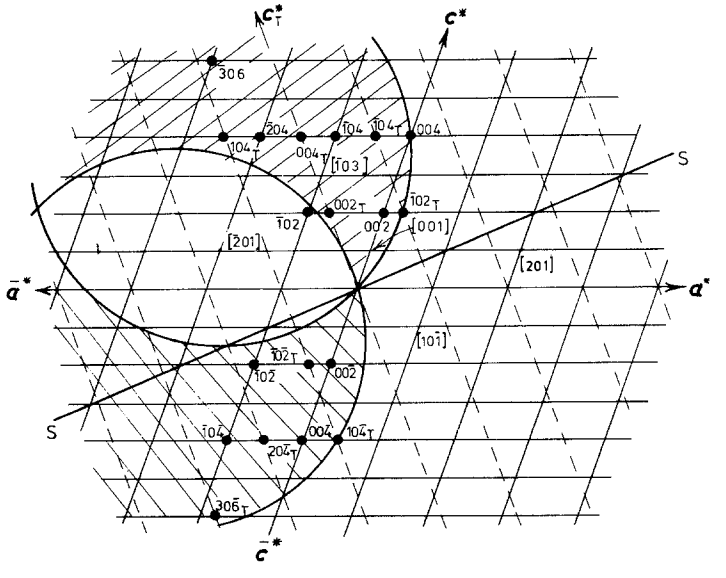

Figure 6 The $h0l$ recprical lattice net twinned about the c-axis. The labelled reflections correspond to those observed in Fig. 5b.

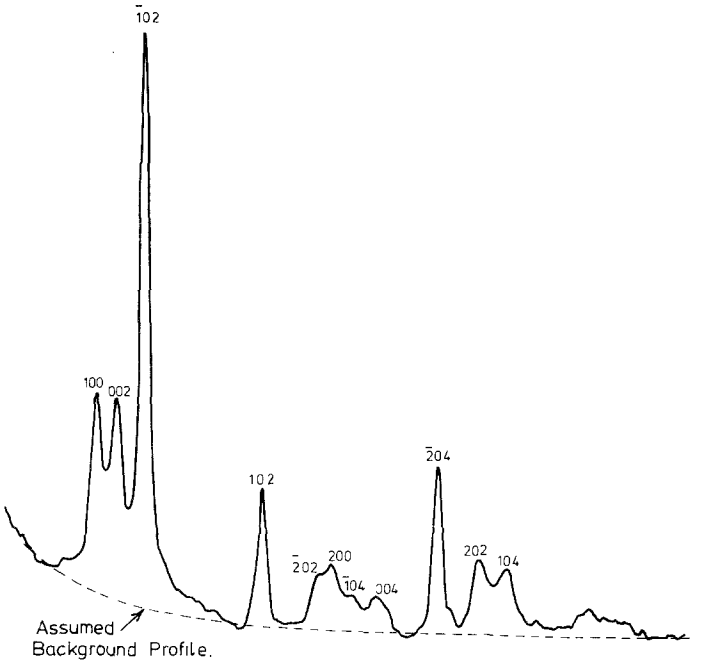

Figure 7 Intensity profile of the zero layer line reflections of Fig. 5a.

intensities of individual reflections, I_0, are proportional to the square of their respective structure factors, F_c^2. Hence the ratio I_0/F_c^2 should be constant. The ratios are listed in Table V for the Mikulski and Boudeulle structures. The values for I_0 are relative rather than absolute. F_c^2 was calculated using the standard equation,

$$F_{hkl} = \sum f_n(\theta) \exp\left[2\pi i\,(hx_n + ky_n + lz_n)\right] \tag{1}$$

where $f_n(\theta)$ is the atomic scattering factor of the nth atom in the unit cell, and $x_n y_n z_n$ are the coordinates of the four identical atoms in each unit cell. The structure factors obtained were corrected for thermal vibrations by multiplying by the Debye–Waller factor and by the Lorentz-polarization factor $[1 + \cos^2(2\theta)/2 \sin(2\theta)]^{1/2}$.

The predicted consistancy in F_c^2/I_0 is far better for the Mikulski structure than for the Boudeulle structure.

One further important qualitative consideration can be made from Fig. 7. The two peaks 102 and $\bar{2}04$ are well separated from other peaks and they sit on a relatively low background. The $\bar{2}04$ peak is clearly more intense than 102. This is as expected from the Mikulski structure. Boudeulle, however, predicts the 102 reflection to be the stronger, with the intensity of the $\bar{2}04$ reflection only 75% of that of 102.

TABLE V Structure factor calculations and measured relative X-ray intensities for SN_x. The numbers in brackets are estimated uncertainties. M Mikulski values, B Boudeulle values

hkl	F_c^2		Observed relative intensities, I_0	$F_c^2/I_0 \times 10$	
	M	B		M	B
100	3640	2910	15 (1.5)	24 (2)	19 (2)
002	2310	2270	11 (2)	21 (4)	21 (4)
$10\bar{2}$	9610	8720	44 (2)	22 (1)	20 (1)
102	1280	1440	6 (0.5)	21 (2)	24 (2)
$20\bar{2}$	880	516	4 (0.5)	22 (3)	13 (3)
200	683	789	3 (0.5)	23 (4)	26 (4)
$10\bar{4}$	364	410	2 (0.5)	18 (6)	21 (6)
204	1530	1090	7 (0.5)	22 (2)	16 (2)
202	1120	1170	4 (0.5)	28 (5)	29 (5)
104	978	1080	4 (0.5)	24 (5)	27 (5)

3.4. Transmission electron microscopy

Fig. 8 shows a typical dark-field image of an $(SN)_x$ TEM strand. Such images show that the strands are of small fibres typically 10–20 nm thick. But finer details down to 2 nm can also be seen. The bright areas in a dark-field image show areas of the same crystal orientation. Typically, these areas vary in size from 2 to 10 nm, and constitute only a fraction of the total volume illuminated. Other parts of the strand could be made to appear bright by tilting up to ± 5° about an axis either parallel or perpendicular to the polymer chain axis. This shows that there is a certain mosaic spread both about the chain axis and perpendicular to it. Other parts of the strand would appear bright only by choosing a different reflection for the dark-field imaging, which indicates that this reflection belongs to a different zone axis pattern and that the crystal is twinned. The TEM work presented is mainly concerned with studying the crystallographic relationship between these different zone axis patterns.

Our work was concentrated on studying the thinnest possible strands that could be prepared. Typical of these is that shown in Fig. 9. The visible part of the strand shows a remarkable length to thickness ratio of 1000 and such strands were neither mechanically twisted nor bent. Selected area diffraction from 1 μm lengths usually contained superimposed patterns, as with those from the larger strands, but now the number in any one pattern was smaller so that the separate zone axes contributing, could be positively identified.

Only in one case was a pattern containing only one zone axis recorded (Fig. 10). It was obtained from a strand 30 nm wide, oriented, as with all those discussed below, with the fibre axis perpendicular to the incident beam. The pattern is indexed according to the $(SN)_x$ β structure, as a [100] pattern. The zero layer line of this pattern lies along the c^*-axis of Fig. 6.

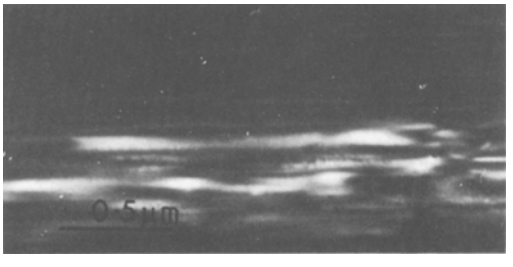

Figure 8 A typical dark-field image of an $(SN)_x$ strand.

Figure 9 A thin $(SN)_x$ strand showing that they could be prepared for TEM observations without significant mechanical damage from twisting or bending. By rotating the strand 45° about its axis it was shown not to be bent.

For the $P2_1/C$ space group, $h0l$ reflections for which $l = 2n + 1$ (n being an integer) are forbidden, as are $0k0$ reflections with $k = 2n + 1$. Fig. 10 shows, however, that such reflections may occur, notably reflections 001, 003, 010 and 030. Dynamic effects may therefore be invoked to account for the presence of such reflections.

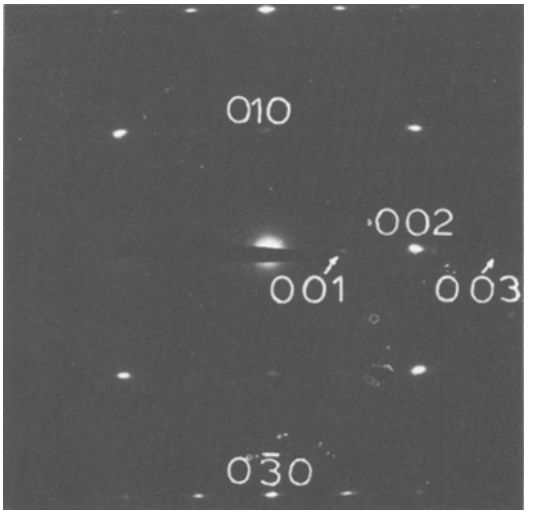

Figure 10 A [100] zone axis pattern from an $(SN)_x$ fibre 30 nm thick.

Alternatively, the 010 and 030 reflections may appear because of small atomic displacements perpendicular to the chain plane. This phenomena is frequenctly observed in biopolymers [7] where forbidden reflections whose vector is perpendicular to a screw axis, often occur.

Fig. 11 shows a diffraction pattern of considerably more complexity. This type of pattern was frequently observed from bigger strands and is typical of diffraction patterns found in the literature and presented there as 001 patterns. We have been able, however, to identify at least three different zone axes in this pattern. The 100 and 010 reflections define a [001] zone axis, the 011 and 010 reflections define a [100] axis, and the 202 and 010 reflections define a $[10\bar{1}]$ axis.

The superposition of [001] and [201] patterns shown in Fig. 12 was also frequently observed. We have also positively identified the superposition of the following diffraction patterns: [201] with $[20\bar{1}]$; [001] with [201] and $[\bar{2}01]$; and finally, [001] with $[10\bar{1}]$ and $[20\bar{1}]$.

It is most likely that the origin of the crystallographic relationship between the superimposed zone axes is that of twinning. The possibility that twisting of the fibres had some effect on this,

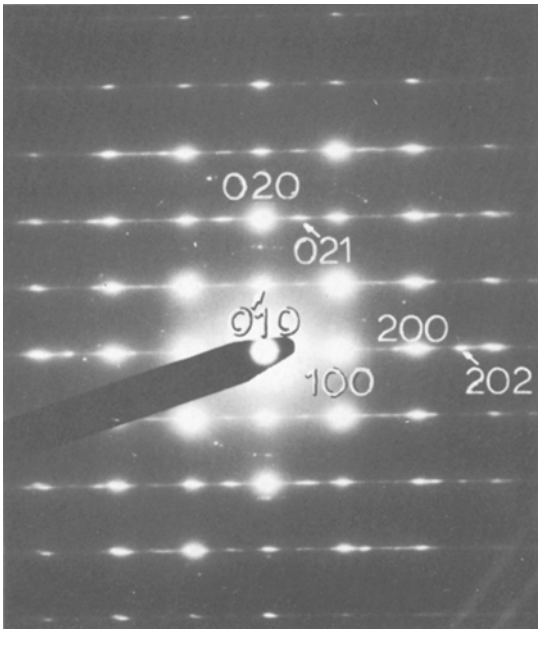

Figure 11 Three superimposed zone axis patterns from a single area of an $(SN)_x$ crystal; [100], [001], $[10\bar{1}]$. The forbidden 001 reflection has been marked in for convenience.

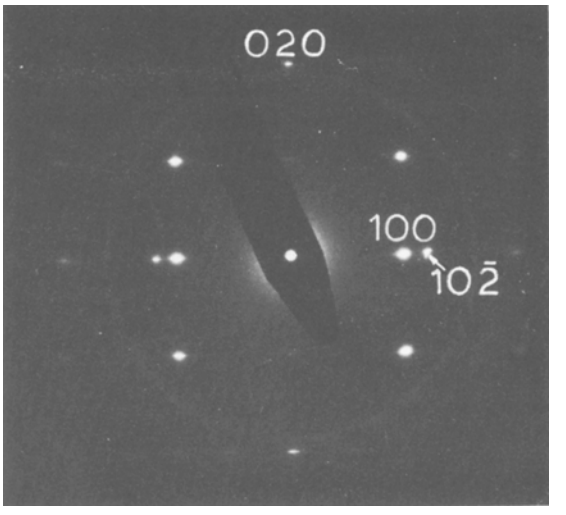

Figure 12 The 100 and 020 reflections define a [001] zone axis, and 102 and 020 define a $[20\bar{1}]$ zone axis.

however, was investigated with the following observations. Firstly, the twist rate needed to result in two zone axes appearing in the same difracting area of one μm diameter would be a minium of $24^\circ\,\mu m^{-1}$. Structurally, this is highly unlikely, though in one case a 200 nm thick fibre was observed to be continuously twisted over a length of 10 μm at a twist rate of $5^\circ\,\mu m^{-1}$. Secondly, if a fibre is continuously twisted, the Ewald sphere will sweep through a large volume in reciprocal space and therefore excite several additional reflections. These reflections were not observed, however.

4. Discussion

We begin from the accepted twin mode observed by Boudeulle and theoretically interpreted by Baughman. In the formation of the $(SN)_x$ phase from the S_2N_2 dimer (Fig. 2b and c) every second plane of the dimer rings in the c_d^* direction, will have to be rotated about the final polymer chain axis so that all the chain planes are parallel. If the first and third planes in Fig. 3b had suffered the rotation instead, the resultant crystal would be the twin shown, the two being related by a mirror plane coincident with the (100) plane of the polymer phase, equivlanet to a 180° rotation about the c-axis. This is the Boudeulle twin. It was commonly observed and is that represented in Fig. 6. This twin mode does not account, however, for any of the additional superposition of patterns listed above.

Further consideration of the polymerization process, as discussed in the introduction, shows that it is not unique, in that either of the two centro-symmetrically related bonds in the S_2N_2 ring may break in forming the $(SN)_x$ chains (Fig. 3), resulting in alternative orientations related by a 180° rotation about an axis perpendicular to the chain plane. This direction is within 2° of the reciprocal lattice direction $(\bar{1}02)^*$. The unit cell relationship, viewed along the *b*-axis, is then as illustrated in Fig. 13 and the corresponding superimposed reciprocal lattice nets in Fig. 14.

If the incident electron beam were now along A0 (Fig. 14) with the Ewald sphere cutting the figure along TT the excited reflections would correspond, in part, to those seen in Fig. 11 accounting for the superposition of [001] with [100]. Further, with the Ewald sphere as drawn, i.e. closer to the [001] matrix zone axis reflections, the matrix reflections would be correspondingly stronger than those from the twin, their deviation parameter from the Bragg condition being smaller. This would account for the anomalously low intensity of the [021] twin reflection compared with the 200 matrix reflection, which, according to structure factor calculation, should have been the stronger.

Similarly, an Ewald sphere intersection along either XX or YY would image both 102 and 202_T reflections (T refers to the twin) in the same pattern giving rise to the superposition of patterns from zone axes $[20\bar{1}]$ and $[10\bar{1}]$ as has been observed.

If we now allow the Boudeulle *c*-axis twin and the $[\bar{1}02]^*$ twin to be contained within the same diffracting volume and construct the resultant superposition of reciprocal lattice nets, we can by similar arguments explain the superposition of the [001] and [201] (Fig. 12), and the [100] and [001] zone axis patterns (Fig. 11).

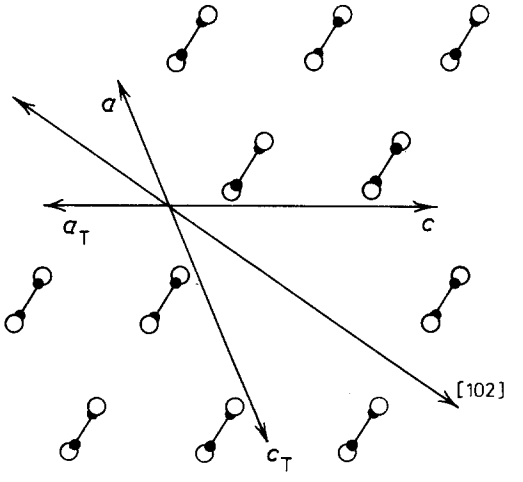

Figure 13 The orientation relationship between the parent crystal and $(102)^*$ twin.

Furthermore, our calculations show that with the existence of a $(\bar{1}02)^*$ twin, the [201] and [001] zone axes are separated by a rotation of 5.2° about the fibre axis. This matches very well tilting experiments which show that the orientations which maximize the reflected intensities from the two patterns are separated by 5 (± 1)°. Despite this separation, the two patterns may be excited simultaneously by virtue of spiking reciprocal lattice points.

Hence, these observations give strong support towards the existence of the proposed $(\bar{1}02)^*$ twin.

Another possible structural modification is obtained by twinning material in the twin 1 orientation (see Fig. 15) about its $(\bar{1}02)^*$ axis to produce a third twin mode, T3. However, though a distinct mode, it produces no additional superpositions of diffraction patterns to those discussed above.

The *c*-axis twinning, twin 1, was explained by Baughman [8] on the basis that in order to preserve the orientation of the two-fold dimer axis during the solid-state polymerization, the polymer twins about an axis parallel to this direction (Fig. 2). Applying the same criterion to the $(\bar{1}02)^*$ twin, we arrive at two alternative orientation relationships between dimer and polymer phases as depicted in Fig. 16. It is required to maintain the twinning axis parallel to the *b*-axis of the dimer. However, since a 180° rotation about the $(\bar{1}02)^*$ is equivalent to a 180° rotation about an axis perpendicular to this direction (which happens to be the $(\bar{2}0\bar{3})^*$ direction), we arrive at the two alternatives in Fig. 16. The dimer–polymer orientation relationship is either such that b_d is parallel to $(\bar{1}02)^*$ (*a* and *c*) or such that b_d is parallel to $(\bar{2}0\bar{3})^*$ (*b* and *c*).

The main difference between the orientation relationship suggested by Baughman and that of the authors is that in our case all the chains of the partially polymerized phase have to be rotated by an approximately equal amount about this chain axis, whereas according to Baughman half the chains undergo a large rotation whilst the other half undergo only a small rotation.

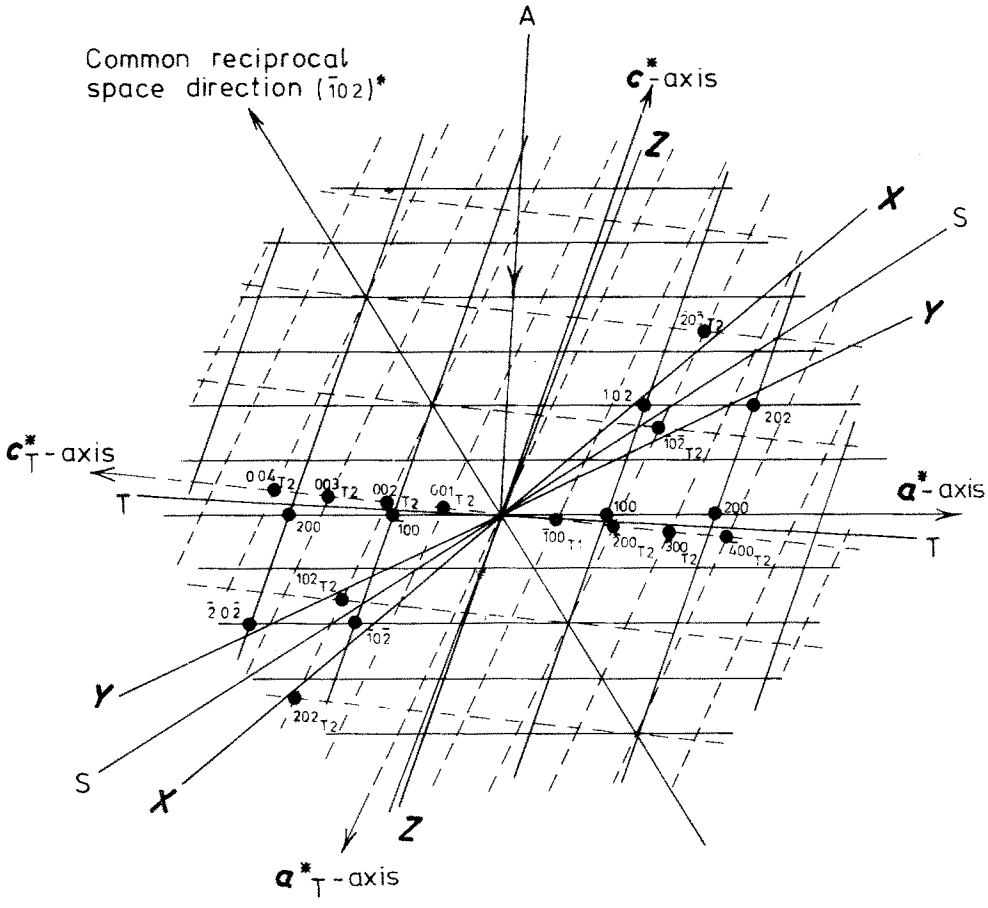

Figure 14 Superimposed reciprocal lattice nets for matrix and $(\bar{1}02)^*$ twin.

For the new orientation relationship proposed, the rotation of partially polymerized chains although being of the same magnitude for all chains, is in the opposite sense for successive planes of chains along the c^*_d direction.

Of the two possible orientation relationships proposed in Fig. 16, relationship b to c is thought more likely than that of a to c for the following reasons. Although a smaller rotation of the partially polymerized chains is required in orientation relationship a to c there is a far better fit of lattice distances in the relationship b to c. In the polymer, the distance between chains in the $(\bar{1}02)$ planes is 0.459 nm. This has to match the spacing of 0.449 nm, along the dimer b-axis for the b–c transformation, or the 0.811 nm spacing along the c^*-axis for the a–c transformation. Conversely, in the perpendicular direction, for the relationship b–c the matching interchain distances are 0.811 nm dimer, with 0.650 nm polymer and for a–c they are 0.449 nm dimer, with 0.605 nm polymer. The better fit of the b–c transformation is clear.

It should be emphasized that both the $(\bar{1}02)^*$

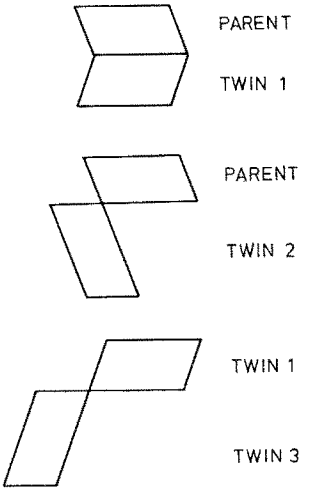

Figure 15 Orientations of the real space unit cells obtained by c-axis, and $(\bar{1}02)^*$ twinning.

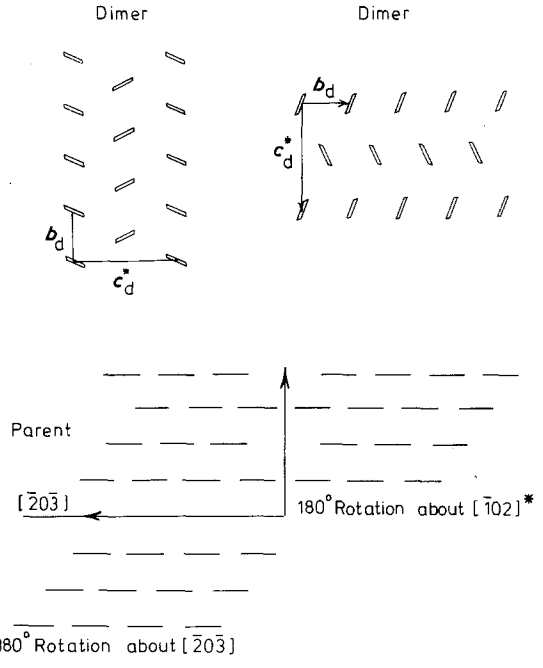

Figure 16 Alternative orientation relationships between dimer and polymer phases to that suggested by Baughman *et al.* [9].

orientation relationship described above and that proposed by Boudeulle are believed to exist; both modes are required to account for the superposition of zone axis patterns presented in the previous sections. We note also that the superpositions observed in the electron diffraction patterns are just those required to produce the diffraction patterns observed in the stationary X-ray diffraction patterns such as shown in Fig. 5.

Fig. 15 shows the relative orientations of the various modes suggested above. Clearly, if each mode was equally populated then any property of the crystal should show five-fold degeneracy. Magnetic critical field superconductivity measurements, however, by Barrett *et al.* [9], show only two-fold degeneracy deriving from the combination of matrix[1] and *c*-axis twinning. This is somewhat surprising as our observations suggest that the $(\bar{1}02)^*$ twin is common and its effects should have been evident in magnetic measurements.

The superposition of the 001 and $10\bar{1}$ patterns in Fig. 11 cannot be explained by the presence of the *c*-axis and $(\bar{1}02)^*$ twins. We have also observed a superposition of $\bar{2}01$ and 001 patterns (not shown) which cannot be explained by these twin modes. It is possible to show that for twinning alone to explain these superpositions of patterns we have to introduce another two twin modes, a $(201)^*$ and a $(\bar{1}03)^*$ mode, respectively. We shall not discuss these modes in any detail, however, as their existence is somewhat ambiguous. It is possible that the accumulated effects of mosaic spread, slightly twisted strands and the *c*-axis and $(\bar{1}02)^*$ twins may result in the superposition of these zone axis patterns.

5. Conclusions

It is concluded that $(SN)_x$ is a material whose structure is highly complex. At least two twin modes exist, the *c*-axis and the $(\bar{1}02)^*$ modes. Bulk crystals are polycrystalline in the sense they are multiply twinned, with crystalline size typically 2 nm × 10 nm. There is a mosaic spread of 10° about both the fibre direction and perpendicular to it.

References

1. M. BOUDEULLE, Ph.D. Thesis, University of Lyon (1974).
2. C. M. MIKULSKI, P. J. RUSSO, M. S. SARAN, A. G. MacDIARMID, A. F. GAVITO and A. J. HEEGER, *J. Amer. Chem. Soc.* 97 (1975) 6358.
3. M. J. COHEN, A. F. GAVITO, A. J. HEEGER, A. G. MacDIARMID, C. M. MIKULSKI, M. S. MORAN and J. KLEPPINGER, *ibid.* 98 (1976) 3844.
4. R. H. BAUGHMAN, private communication (1977).
5. J. STEJNY, J. DLUGOSZ and A. KELLER, *J. Mater. Sci.* 14 (1979) 1291.
6. R. H. BAUGHMAN, R. R. CHANCE and J. COHEN, *J. Chem. Phys.* 64 (1976) 1869.
7. E. D. T. ATKINS, D. H. ISAAC, I. A. NIEDUSZYNSKI, C. F. PHELPS and J. K. SHEEHAN, *Polymer* 15 (1974) 263.
8. R. H. BAUGHMAN, *J. Polymer Sci. Polymer Ed.* 12 (1974) 1511.
9. P. BARRETT, G. M. BRIMLOW, W. G. HERRENDEN-HARKER and M. G. PRIESTLY, *J. Phys. F Meta. Phys.* in press.

Received 2 April 1981
and accepted 22 March 1982